1990-09

Free Surface Effects on the Near-Inertial Ocean Current Response to a Hurricane

Shay, Lynn K.

Journal of Physical Oceanography, Vol. 20, September 1990, pp. 1405-1424.
http://hdl.handle.net/10945/46748

Free Surface Effects on the Near-Inertial Ocean Current Response to a Hurricane

LYNN K. SHAY

Division of Meteorology & Physical Oceanography, Rosenstiel School of Marine & Atmospheric Science, University of Miami, Miami, Florida

SIMON W. CHANG

Atmospheric Physics Branch, Naval Research Laboratory, Washington, D.C.

RUSSELL L. ELSBERRY

Department of Meteorology, U.S. Naval Postgraduate School, Monterey, California

(Manuscript received 8 September 1989, in final form 12 March 1990)

ABSTRACT

During the passage of hurricane Frederic in 1979, four ocean current meter arrays in water depths of 100–950 m detected both a baroclinic and a depth-independent response in the near-inertial frequency band. Although the oceanic response was predominately baroclinic, the hurricane excited a depth-independent component of 5–11 cm s^{-1}.

The origin and role of the depth-independent component of velocity is investigated using a linear analytical model and numerical simulations from a 17-level primitive equation model with a free surface. Both models are forced with an idealized wind stress pattern based on the observed storm parameters in hurricane Frederic. In an analytical model, the Green's function (K_0) is convolved with the wind stress curl to predict a sea surface depression of approximately 20 cm from the equilibrium position. The near-inertial velocities are simulated by convolving the slope of the sea surface depression with a second Green's function. The barotropic current velocities rotate inertially with periods shifted above the local inertial period by 1%–2% and the maximum amplitude of 11 cm s^{-1} is displaced to the right of the track at $x = 2R_{max}$ (radius of maximum winds).

The free surface depression simulated by the primitive-equation model is also about 18–20 cm. The primitive equation model simulations indicate that the vertical mean pressure gradient excites 10–11 cm s^{-1} depth-averaged currents at $x = 3R_{max}$. The net divergence and convergence of the horizontal velocities induces vertical deflections of the sea surface. The spatial pattern of the barotropic amplitudes simulated by the numerical and analytical models differ by less than 2 cm s^{-1} in the region $0 < x < 4R_{max}$, which suggests that the barotropic response to the passage of a moving hurricane is governed by linear processes.

1. Introduction

The passage of a tropical cyclone or an atmospheric front excites energetic ocean currents as the wind stress injects momentum into the mixed layer. Although atmospheric forcing events excite currents and waves on a variety of space and time scales, ocean current and temperature measurements from moored current meter arrays indicate that the predominant response is in the near-inertial waveband (Pollard 1970). The near-inertial current and temperature oscillations excited by the passage of hurricanes have generally been observed at only a few vertical levels at limited points in space (Mayer et al. 1981; Brooks 1983; Shay and Elsberry 1987; Brink 1989). These near-inertial oscillations have 1 m s^{-1} mixed layer current amplitudes and the frequencies are shifted above the local inertial frequency by 1%–20%.

Shay and Elsberry (1987, hereafter referred to as SE) analyzed current and temperature time series from four moored, subsurface current meter arrays at distances of 3–5 radius of maximum winds (R_{max}) from the track of hurricane Frederic in 1979 (Fig. 1). Three of these subsurface, current meter arrays were deployed by the U.S. Naval Oceanographic Office and were instrumented with 11 Aanderaa RCM-5 current meters. The subsurface arrays were configured with a flotation device (a subsurface buoy) located at 20 m below the surface or 1 m above the mixed layer current meter (not on the surface as described in Cooper and Thompson 1989). Although Aanderaa current meters are susceptable to measurement errors (Beardsley et al. 1981), this type of array design attempts to minimize contamination of the current meter records by the orbital velocities induced by surface waves (Sanford et al. 1987).

Corresponding author address: Dr. Lynn K. Shay, RSMAS, Division of Meteorology and Physical Oceanography, University of Miami, 4600 Rickenbacker Causeway, Miami, Florida 33149-1090.

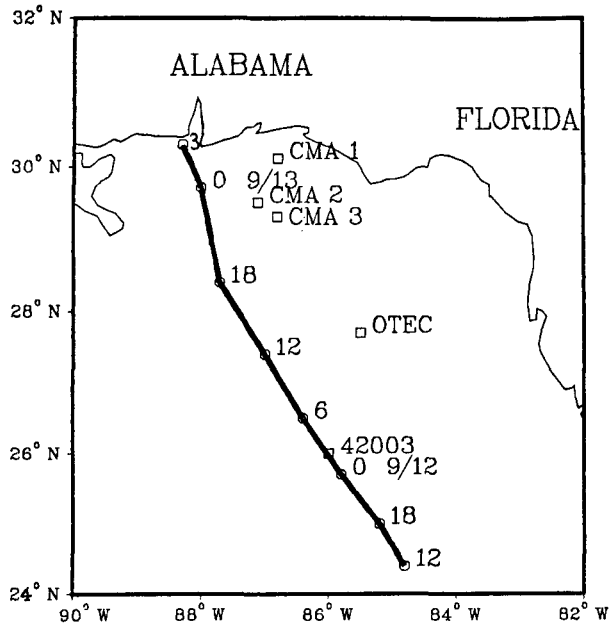

FIG. 1. The path (circles) of hurricane Frederic in the northern Gulf of Mexico (Hebert 1979) beginning 12 UTC 11 Sep and ending 03 UTC 13 Sep 1979. The boxes depict the NOAA data buoy 42003, the OTEC and three NAVOCEANO current meter arrays (CMA 1, 2 and 3).

The observed ocean currents indicate the excitation of energetic near-inertial oscillations throughout the water column (Fig. 2). The increase in currents was first detected about 8–9 h before the point of closest approach. Mixed layer currents oscillated with magnitudes of about 90 cm s^{-1} whereas thermocline amplitudes were 25–30 cm s^{-1}. Even at an Ocean Thermal Energy Conversion (OTEC) site at $x = 5R_{max}$, an increase in the current amplitudes was detected at 950 m depth (not shown). Brooks (1983) found similar increases in the currents amplitudes throughout the water column during and subsequent to the passage of hurricane Allen. SE demodulated the current meter observations and expanded the data into a depth-averaged current and the first two baroclinic modes. A possible criticism of the SE study is that the low mode amplitudes may include aliased higher-order baroclinic modes that could not be resolved by limited vertical sampling of the moorings. Thus, some uncertainty remains as to whether the calculated near-inertial depth-averaged current is real and is associated with the free-surface effects, or is it an artifact of limited vertical sampling?

Theoretical treatments of the ocean response to storms have been developed for the directly forced region, or near-field (Kajiura 1958; Geisler 1970; Ichiye 1976), and for the far-field (Gill 1984). Kajiura (1958) studied the combined baroclinic and barotropic response of the ocean to a moving hurricane using Green's functions. In a similar treatment, Geisler (1970) used a linear, two-layer model to demonstrate that the oceanic wavelengths (Λ) induced by a moving hurricane are proportional to the product of the storm translation speed (U_h) and the inertial period (IP). If the storm translation speed (U_h) is greater than the first mode phase speed (c_1), the oceanic response in the wake is dominated by baroclinic, near-inertial oscillations. Since the phase speed of the barotropic mode (c_0) will nearly always exceed the storm translation speed (except in very shallow water), there may also be a barotropic response. Although Geisler's solution for the barotropic response applied to the steady-state solution, there is a time-dependent barotropic response induced by the gradients in the sea-surface elevation.

The focus here is the origin and role of the depth-averaged current response induced by the passage of a hurricane, and especially the depth-independent current oscillation that has a frequency in the near-inertial waveband. This mode is part of the barotropic trough discussed in Geisler (1970) and differs from the elevation of the sea surface associated with the storm surge

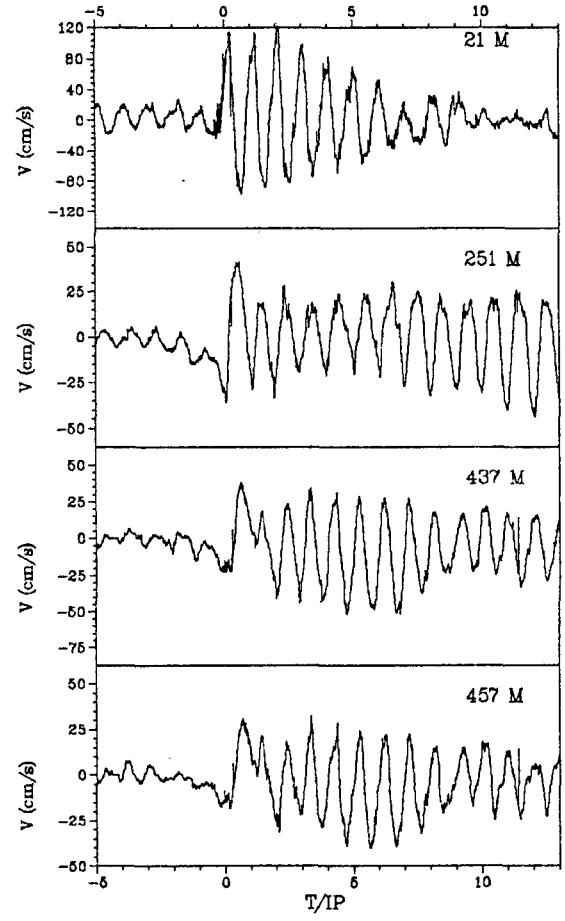

FIG. 2. Along-track velocity time series at CMA3 from 7 Sep to 25 Sep 1979. Time $t = 0$ corresponds to the time of closest approach of hurricane Frederic at 21 UTC 12 Sep.

due to the inverted barometric effect. A fundamental distinction is that the barotropic trough occurs in the storm's wake, whereas the storm surge moves with the storm center.

The Chang and Anthes (1978), Adamec et al. (1981), Hopkins (1982), Price (1983) and Greatbatch (1983) numerical models of the baroclinic response to a translating hurricane, had a rigid lid at the sea surface, which eliminated the barotropic inertial response. Hopkins (1982) simulated the dynamic response to a model hurricane moving at the same translation speed as Frederic and found that the simulated mixed-layer currents agreed well with the Frederic observations. However, the thermocline currents were underestimated by 12–15 cm s^{-1} in the model. This discrepancy between the simulations and observations was hypothesized to be due to the neglect of the free surface.

Price (1983) examined the baroclinic response in the wake of a hurricane using a multilayered primitive equation model and observations acquired during hurricane Eloise at the EB-10 buoy. Since the depth of the ocean exceeded 4000 m in that region, a rigid lid was imposed in the model. The amplitudes and phases of the simulated currents agreed fairly well with the observed ocean currents at 53 m.

Chang (1985) was the first to model both the baroclinic and barotropic response to a hurricane. Because the barotropic mode propagates so quickly in a free-surface model of the deep ocean (2000 m), small time steps must be taken to satisfy computational stability. This computational problem was circumvented by introducing a mode-splitting technique. Cooper and Thompson (1989) used a multilayer, primitive equation model with a free surface and simulated the ocean response to hurricane Frederic. Although the response was predominantly baroclinic (~80%), they found that the barotropic trough depression was about 20 cm in the wake of hurricane Frederic.

The effect of the free surface on the near-inertial ocean current response is investigated here using simulations from linear analytical and primitive equation models. In the analytical model, the ocean is forced by the wind stress curl and the sea-surface elevation is obtained by convolving the wind stress curl with a modified Bessel function (K_0). A geostrophic current is obtained from the steady-state solution. To form a time-dependent solution, a second Green's function is found by solving the shallow water equations. This second Green's function is convolved with the spatial gradients of the sea surface slope to form a time-dependent barotropic current response. The frequency and amplitude of the barotropic mode are calculated from this function.

Simulations from the 17-level, primitive equation model indicate that both geostrophic and near-inertial currents are induced by the free-surface depression. Near-inertial amplitudes are isolated by demodulating the simulated velocities at a carrier frequency and calculating the clockwise-rotating components (Mooers 1973). The depth-averaged near-inertial current is compared to the SE observations from hurricane Frederic and the analytical model.

2. Forced model

Kajiura (1958) examined the displacement of the free surface induced by a hurricane with both wind stress and atmospheric pressure gradients. However, explicit relationships for the time-dependent, ocean current velocities were not derived. The three-dimensional velocity structure associated with the baroclinic response was derived in Shay et al. (1989) by extending the two-layer model of Geisler (1970) to a continuously stratified fluid following Kundu and Thomson (1985). In this section, the ocean's barotropic current response in the near-inertial frequency band is treated using the forced, shallow water equations.

a. Linear theory

A linear, inviscid homogeneous ocean with a flat-bottom is assumed. The equations for a hydrostatically balanced ocean on an f-plane are

$$\frac{\partial u}{\partial t} - fv = -g\frac{\partial \eta}{\partial x} + \frac{\tau^x}{H\rho_0}, \tag{1}$$

$$\frac{\partial v}{\partial t} + fu = -g\frac{\partial \eta}{\partial y} + \frac{\tau^y}{H\rho_0}, \tag{2}$$

$$\frac{\partial \eta}{\partial t} + H\left[\frac{\partial u}{\partial x} + \frac{\partial v}{\partial y}\right] = 0, \tag{3}$$

where η is the sea-surface elevation and H is the ocean depth. The remainder of the variables are as defined in other treatments. The storm surge associated with the low atmospheric pressure center is outside the scope of this paper and will be neglected.

Substituting (1) and (2) into (3), the governing equation for the sea-surface elevation is

$$\left[\frac{\partial^2}{\partial t^2} + f^2 - c_0^2\left(\frac{\partial^2}{\partial x^2} + \frac{\partial^2}{\partial y^2}\right)\right]\eta = fH\int_{-\infty}^{\infty} \nabla \times \tau dt + H\nabla \cdot \tau \tag{4}$$

In the unforced case, equation (4) can be simplified into the dispersion relation for free barotropic motion

$$\sigma^2 = f^2 + c_0^2 K^2,$$

where σ is the wave frequency and $K^2 = k^2 + l^2$ is the total horizontal wavenumber. These waves have O(10^4 km) wavelengths, rotate clockwise with frequencies close to the inertial frequency and propagate very quickly since the phase speed $c_0 = \sqrt{gH}$ is typically O(100 m s^{-1}) (Gill 1982).

b. Model of the wind stress

A common representation of a hurricane wind and wind stress distribution is the Rankine vortex (Chang and Anthes 1978). The radial and tangential wind-stress components are given by

$$\tau_r, \tau_\theta = -|\tau_{rm}|, |\tau_{\theta m}| \times \begin{cases} \dfrac{r}{R_{\max}}, & r < R_{\max} \\ \dfrac{(R_{\text{out}} - r)}{(R_{\text{out}} - R_{\max})}, & R_{\max} < r < R_{\text{out}} \\ 0, & r > R_{\text{out}}, \end{cases}$$

where $R_{\max}$ (radius of maximum winds) = 30 km and R_{out} (radius to the outer edge of the hurricane) = 200 km. Since the maximum wind stress in Frederic ranged from 30–44 dyn cm^{-2} (Black 1983), the value specified in these simulations if 33 dyn cm^{-2}. Although the wind stress curl exceeds 220×10^{-7} cm s^{-2} within $\pm R_{\max}$, the decrease in curl is very rapid so that its length scale is $2R_{\max}$ (60 km for Frederic). Since hurricane Frederic had an inflow angle of about 20°, the maximum stress divergence is about 40×10^{-7} cm s^{-2}.

c. Sea-surface depression

The motivation for this section is to demonstrate that the sea-surface depression (Geisler 1970) is driven by the wind-stress curl and stress divergence. Because the hurricane is assumed to be moving with speed U_h in the $+y$ direction, the local time derivative may be transformed into a space derivative. The differential operator on the left side of (4) can be expressed as

$$L_2 = -\left(1 - \frac{U_h^2}{c_0^2}\right)\frac{\partial^2}{\partial y^2} - \frac{\partial^2}{\partial x^2} + \alpha_0^2$$

where α_0 is the inverse deformation radius (f/c_0) associated with the barotropic mode, which is O(10^3 km). Since $c_0 > U_h$, the differential operator is elliptical, and substituting this expression into (4) yields

$$L_2\eta = -\frac{fH}{U_h c_0^2}\int_{-\infty}^{\infty} \nabla \times \tau dy + \frac{H}{c_0^2}(\nabla \cdot \tau).$$

A nondimensional coordinate system is adopted from Geisler (1970)

$$y' = \left(1 - \frac{U_h^2}{c_0^2}\right)^{-1/2} \alpha_0 y, \; x' = \alpha_0 x,$$

which transforms the operator into

$$L_2' = \alpha_0^2\left(\frac{\partial^2}{\partial y'^2} + \frac{\partial^2}{\partial x'^2} - 1\right).$$

The governing expression for the sea-surface elevation becomes

$$L_2'\eta = -\frac{H}{fU_h}\int_{-\infty}^{\infty} \nabla \times \tau dy + \frac{H}{f^2}(\nabla \cdot \tau). \quad (5)$$

The solution of the partial differential operator (L_2') involves double Fourier transforming and inverting an integral equation. The fundamental solution to the inversion of the integral is represented by a Green's function that is a modified Bessel's function of order 0 (Geisler 1970)

$$\frac{K_0[(y'^2 + x'^2)^{1/2}]}{2\pi} H(y' + x').$$

The modified Bessel function is appropriate because a hurricane can be approximated by an axisymmetric point source translating over the ocean and $H(y' + x')$ represents a unit step function.

To solve for the sea-surface displacement, the Green's function is convolved with the wind stress curl and stress divergence integrated over all source points $(\bar{x}', \bar{y}')$ within the region of forcing

$$\eta = -\frac{1}{2\pi f U_h}\int_{-\infty}^{\infty}\int \left[\int_{-\infty}^{\infty} \nabla \times \tau dy\right] K_0(r') d\bar{x}' d\bar{y}' - \frac{1}{2\pi f^2}\int_{-\infty}^{\infty}\int (\nabla \cdot \tau) K_0(r') d\bar{x}' d\bar{y}'. \quad (6)$$

The modified Bessel function represents the kernel in the convolution and the argument is given by

$$r'^2 = \frac{1}{\alpha_0^2}\left[\left(1 - \frac{U_h^2}{c_0^2}\right)(\bar{y}' - y')^2 + (\bar{x}' - x')^2\right].$$

In these convolutions, the limits of integration extend to $\pm 6R_{\max}$ as in Shay et al. (1989).

Geisler (1970) did not numerically evaluate the free-surface depression or the barotropic trough induced by the passage of a hurricane. The sea-surface depression (Fig. 3) is determined by convolving the wind-stress forcing with the modified Bessel function as in (6). Although the combination of the wind stress curl and divergence depresses the sea surface by about 22 cm below the undisturbed level, most of the sea-surface depression (18 cm) is induced by the wind stress curl. For an inflow angle of 20°, the contribution by the stress divergence term is approximately 4 cm and is in phase with the contribution of the wind stress curl to the depression. The depression extends well beyond the $\pm 6R_{\max}$ limits and decreases as $e^{-|y|}$, which follows from an asymptotic expansion of K_0.

d. Horizontal velocities

The sea-surface slope induced by the wind stress curl and stress divergence excites both a steady solution and

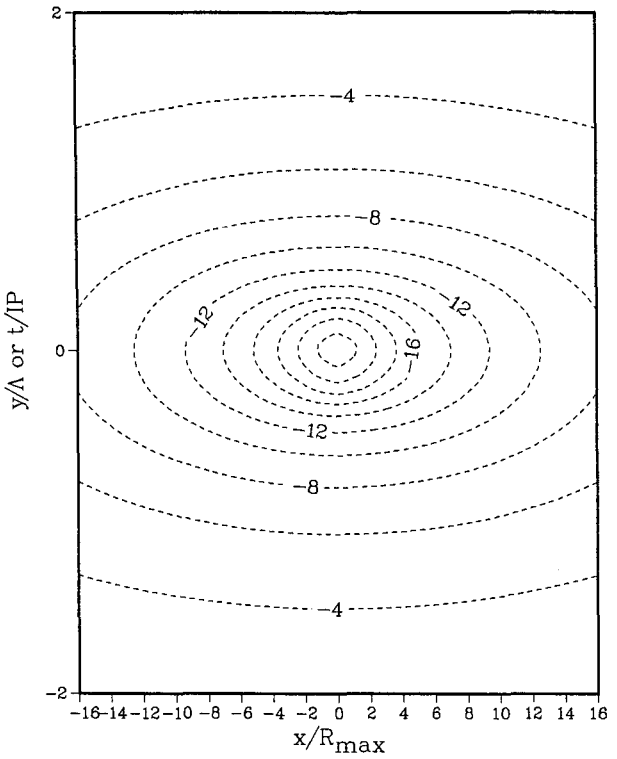

FIG. 3. Sea-surface depression (cm) induced by the wind stress curl and divergence from the analytical model with a contour interval of 2 cm. The axes are scaled in terms of the radius of maximum winds R_{max} (30 km) and the near-inertial wavelength Λ (580 km). The storm is moving northward along $x = 0$ at 6.5 m s^{-1}.

time-dependent velocity that rotates inertially. The governing equations for the barotropic horizontal velocities are given in Pedlosky (1979) as

$$\left\{\frac{\partial^2}{\partial t^2} + f^2\right\}u = -g\left\{\frac{\partial^2\eta}{\partial x \partial t} - f\frac{\partial \eta}{\partial y}\right\},$$

$$\left\{\frac{\partial^2}{\partial t^2} + f^2\right\}v = -g\left\{\frac{\partial^2\eta}{\partial y \partial t} - f\frac{\partial \eta}{\partial x}\right\}.$$

Notice that wind stress terms do not explicitly appear in these expressions because only the baroclinic current is directly forced by the wind stress (Shay et al. 1989). The forcing terms for the time-dependent barotropic current are the spatial gradients of the sea-surface depression. The steadily moving storm assumption (not steady-state) allows the equations to be transformed into

$$\left[\frac{\partial^2}{\partial y^2} + \frac{f^2}{U_h^2}\right]u = -\frac{g}{U_h^2}\left\{U_h\frac{\partial^2\eta}{\partial x \partial y} - f\frac{\partial\eta}{\partial y}\right\} = F(x, y),$$

$$\left[\frac{\partial^2}{\partial y^2} + \frac{f^2}{U_h^2}\right]v = -\frac{g}{U_h^2}\left\{U_h\frac{\partial^2\eta}{\partial y^2} + f\frac{\partial\eta}{\partial x}\right\} = G(x, y). \quad (7)$$

To solve (7), the right side is replaced by a dirac delta function to represent a concentrated forcing function. The contributions of η_x and η_y represent the geostrophic velocity components that are subtracted from the other two terms. The equations are Fourier transformed in y and inverted to form an integral equation

$$\frac{1}{2\pi}\int_0^\infty \frac{e^{-ily}\,dl}{(a^2 - l^2)}$$

where $a = f/U_h$. Notice that a, which is the product of the translation speed (U_h) of the hurricane and the Inertial Period (IP), is the inverse of the horizontal wavelength $(\Lambda)^{-1}$ of the baroclinic response. This integral is recast into the cosine transforms and can be found in Erdelyi et al. (1954)

$$\frac{1}{2\pi}\int_0^\infty \frac{e^{-ily}\,dl}{(a^2 - l^2)} = \frac{1}{4a}\sin(ay),$$

which is a fundamental solution to the second-order differential operator. The fundamental solution is convolved with the forcing functions $[F(\bar{x}, \bar{y}), G(\bar{x}, \bar{y})]$ and integrated over the source region. These solutions are subject to radiation boundary conditions (Lighthill 1967) such that $u, v(\pm\infty) \to 0$. To satisfy radiation conditions, the damping term is $1/\sqrt{y'}$ (where $y' \approx y\alpha_0$) which was also found by Ichiye (1976). Note that the current velocities become unbounded and physically unrealistic when $y' < 1$. Consequently, the convolutions involve a term in the region of $y' \leq 1$ and the damped solution extends beyond $y' > 1$. Thus, the barotropic velocities are

$$u(x, y) = \begin{cases} \dfrac{g}{4f}\displaystyle\int_{-\infty}^{0} \sin[a(\bar{y} - y)]F(\bar{x}, \bar{y})\,d\bar{y}, \\ \qquad\qquad y' \leq 1 \\ \dfrac{1}{\sqrt{y'}}\dfrac{g}{4f}\displaystyle\int_{-\infty}^{0} \sin[a(\bar{y} - y)] \\ \qquad \times F(\bar{x}, \bar{y})\,d\bar{y}, \quad y' > 1, \end{cases} \quad (8a)$$

$$v(x, y) = \begin{cases} \dfrac{g}{4f}\displaystyle\int_{-\infty}^{0} \sin[a(\bar{y} - y)]G(\bar{x}, \bar{y})\,d\bar{y}, \\ \qquad\qquad y' \leq 1 \\ \dfrac{1}{\sqrt{y'}}\dfrac{g}{4f}\displaystyle\int_{-\infty}^{0} \sin[a(\bar{y} - y)] \\ \qquad \times G(\bar{x}, \bar{y})\,d\bar{y}, \quad y' > 1. \end{cases} \quad (8b)$$

The most striking feature (Fig. 4) is the 11 cm s^{-1} barotropic currents to the right of the storm track at $x = 2R_{max}$. In modeling studies of the ocean's baroclinic

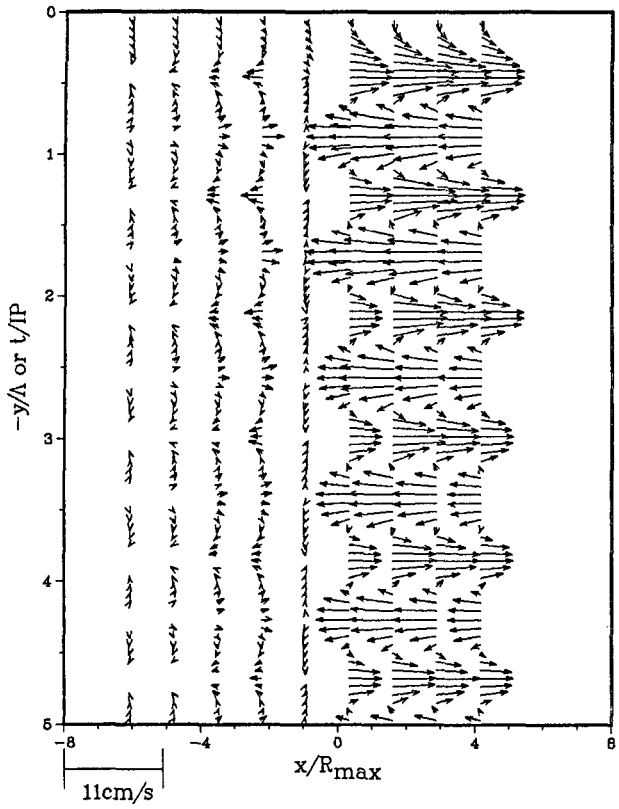

FIG. 4. The barotropic current (cm s^{-1}) simulated from the analytical model. The length of the vectors is proportional to the magnitude of the current according to the scale along the x-axis. The axes are scaled as in Fig. 3.

response to a hurricane, maximum baroclinic currents also are displaced to the right of the track by 2–3R_{max} by nonlinear advection (Chang and Anthes 1978) or resonance excitation (Price 1983). The wavelength of the barotropic oscillations is shifted above the wavelength of the baroclinic response (Λ) by an amount proportional to $(1 - U_h^2/c_0^2)^{-1/2}$. In a 610 meter deep ocean as in the Frederic observations of SE, the frequency is shifted above the local inertial frequency by about 1%. The decay of the barotropic current follows $1/\sqrt{y\alpha_0}$ which is the same rate of damping as the baroclinic response (Geisler 1970). Therefore, some characteristics of the forced barotropic currents on an f-plane are similar to the forced baroclinic currents. Although the observed response in the oceanic wake of hurricane Frederic is primarily baroclinic, the 11 cm s^{-1} near-inertial barotropic component is about 30% of the total current response after one IP and 10%–15% after 3 IP (SE).

e. Model sensitivity

A series of numerical experiments was performed to assess the sensitivity of the linear model to variations in the parameters (Table 1). The depth is varied from 300 m to 4000 m to represent the shelf break region and the deep ocean, respectively. The corresponding variations in the phase speed range from 54 m s^{-1} to nearly 200 m s^{-1}, which also changes the wavelength of the response because of the factor $(1 - U_h^2/c_0^2)$. The amplitude of the barotropic current decreases as the ocean depth increases, which explains the small amplitude of the barotropic current in the open ocean case (Brink 1989).

TABLE 1. Summary of key parameters in linear model simulations for the barotropic response.

Depth (m)	c_0 (m s^{-1})	α_0^{-1} (km)	η_{max} (m)
300	54	766	30
610	77	1092	22
1000	99	1405	18
2000	140	1985	12
4000	198	2808	8

To allow a direct comparison with the observations, the simulated currents are demodulated at a carrier frequency of $1.01f$ to determine the amplitudes of the near-inertial currents. At $x = 3R_{max}$, the initial amplitude of the barotropic current in 300 m of water exceeds 20 cm s^{-1}, whereas the maximum amplitude is only about 2 cm s^{-1} for depth of 4000 m, (Fig. 5). For a depth of 610 m as in the hurricane Frederic arrays of SE, the amplitudes at $x = 0$ and $x = 3R_{max}$ are 6 and 11 cm s^{-1}, respectively (a detailed comparison is shown below). The amplitudes of the barotropic currents in the 2000 and 4000 m depth experiments are significantly less than in the shallow water cases. Even though these results suggest that a barotropic current can be excited in the deep ocean by a moving hurricane, it is not clear that such a weak response can be detected by current meters (Beardsley et al. 1981).

f. Comparison to observations

At $x = 3R_{max}$, the maximum amplitudes of the observed and simulated barotropic velocities are about 10–12 cm s^{-1} over the first 2 IP (Fig. 6), and are significantly above the amplitudes that can be resolved by the current meters. Except for the 5 cm s^{-1} minima near 1 IP, the simulated and observed amplitudes are within 2 cm s^{-1}. Although the time series is relatively short, the predicted rate of decay also appears to be realistic based on the observational evidence. The 2 cm s^{-1} difference in Fig. 6b indicates that the vertical aliasing of higher order baroclinic modes is small and would be within the noise level of most current meter measurements. More importantly, the calculated depth-averaged current in hurricane Frederic (SE) is not an artifact of limited vertical sampling; rather, the current is associated with the depression of the sea surface. Therefore, the analytical model and observations indicate that hurricane Frederic excited a barotropic response in the near-inertial waveband with initial amplitudes of approximately 11 cm s^{-1}.

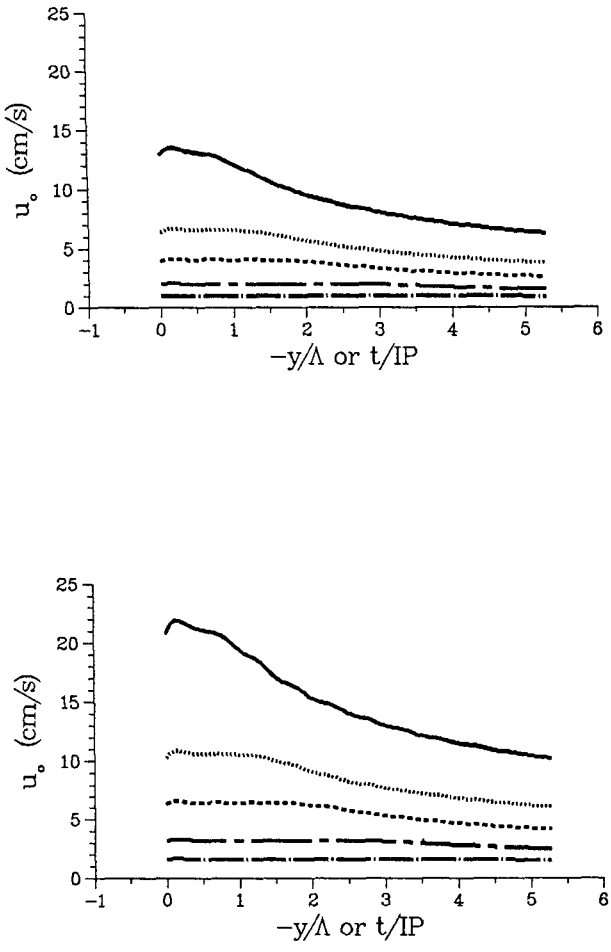

FIG. 5. Simulated amplitudes of the barotropic current induced by a hurricane at $x = 0$ (upper panel) and $x = 3R_{max}$ (lower panel) moving over an ocean with depths of 300 m (solid), 610 m (dot), 1000 m (dash), 2000 m (chain-dash) and 4000 m (chain-dot). The abscissa is scaled in terms of the near-inertial wavelength Λ.

used in Chang (1985) for an axisymmetric model except that these are in Cartesian coordinates

$$\frac{\partial u}{\partial t} = -u\frac{\partial u}{\partial x} - v\frac{\partial u}{\partial y} - w\frac{\partial u}{\partial z} - \frac{1}{\rho_0}\frac{\partial p}{\partial x} + fv + K_z(u) + K_h(u),$$

$$\frac{\partial v}{\partial t} = -u\frac{\partial v}{\partial x} - v\frac{\partial v}{\partial y} - w\frac{\partial v}{\partial z} - \frac{1}{\rho_0}\frac{\partial p}{\partial y} - fu + K_z(v) + K_h(v),$$

$$\frac{\partial \rho}{\partial t} = -u\frac{\partial \rho}{\partial x} - v\frac{\partial \rho}{\partial y} - w\frac{\partial \rho}{\partial z} + K_z(\rho) + K_h(\rho),$$

$$\frac{\partial u}{\partial x} + \frac{\partial v}{\partial y} + \frac{\partial w}{\partial z} = 0,$$

$$\frac{\partial p}{\partial z} + \rho g = 0, \qquad (9)$$

3. Numerical model description

Since previous ocean modeling studies have used ocean depths greater than 1000 m, the barotropic inertial response has been neglected by imposing a rigid lid at the sea surface. Although the observations and the analytical simulations demonstrate that the wake of a moving hurricane has a significant barotropic current, a more sophisticated model is required to isolate key physical mechanisms involved in the barotropic response.

a. Governing equations

A three-dimensional nonlinear, primitive equation model with a free surface and flat bottom has been developed to simulate the baroclinic and barotropic response to hurricane passage. The ocean is assumed to be hydrostatic, incompressible and on an f-plane at 29°N. The governing equations are similar to those

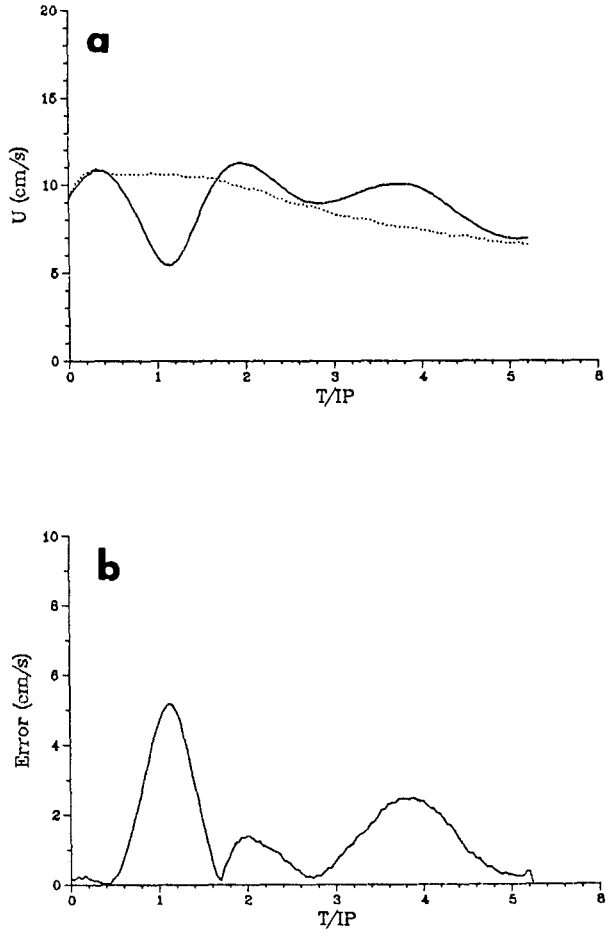

FIG. 6. (a) Amplitudes of the observed barotropic current (solid) at CMA3 in hurricane Frederic (SE) and the barotropic current (dashed) from the analytical model at $x = 3R_{max}$ and (b) the difference between the observed and simulated amplitudes. Notice the scale of the ordinate in (b) is half that of (a).

where the terms K_z and K_h are the turbulent eddy diffusivities in the vertical and horizontal directions respectively.

b. Model grid and storm

A staggered Arakawa-C grid (Haltiner and Williams 1980) is used with grid intervals (Δx, Δy) of 20 km. The C grid has been shown to produce realistic phase and group velocities in the geostrophic adjustment process (Schoenstadt 1977). With 201 × 51 horizontal gridpoints, the model domain is 4000 × 1000 km with cyclic boundary conditions on the east and west sides and Neumann conditions on the north and south boundaries. A vertical grid with 17 levels is stretched for higher resolution in the upper ocean (Δz = 10 m) and lower resolution (Δz = 80 m) below the thermocline (see Fig. 2 in Chang 1985). The total depth (H) is 610 m. Since the focus of this study is on the effect of the free surface on the response to hurricane Frederic, variations in bottom topography are ignored. The slope mode model of Lai and Sanford (1984) used in SE and the primitive-equation model of Cooper and Thompson (1989) show that variations in the bottom topography affect the oceanic response in both the subinertial and near-inertial wave bands.

The model storm is represented by a Rankine vortex using the parameters observed in Frederic (see Table 2). The center of the hurricane starts at 400 km west of the eastern boundary and moves westward at 6.5 m s^{-1} to approximately 500 km east of the western boundary during the 132 h integration. Careful examination of the fields indicates that no significant wave energy reenters the domain through the cyclic boundaries. To simplify comparisons with the current meter observations in Frederic, the simulated data are rotated into a coordinate system with the storm moving to the north. Since the numerical model is on an f-plane, beta-dispersion of inertial waves (Anderson and Gill 1979) is not possible.

c. Mode splitting

A rapidly moving barotropic mode will be excited since the primitive equation model includes a free surface. Thus, a special time-integration is required. To maintain numerical stability, the Courant-Frederichs-Lewy condition is

$$\frac{c_n \Delta t}{\Delta x} < \sqrt{2},$$

where c_n is the largest phase speed to be resolved in the model. For a barotropic mode in 610 m of water, the phase speed (c_0) is 77 m s^{-1}, whereas the phase speed of the first baroclinic mode is 3 m s^{-1}. For a grid spacing (Δx) of 20 km, the maximum time steps would be 267 and 6667 s for the barotropic and first baroclinic modes, respectively. Hence, 25 time steps are required to integrate the barotropic mode for every baroclinic mode time step.

Chang (1985) introduced a mode-splitting technique by subtracting the mean weight of the fluid (hydrostatic approximation) from the total pressure to form a relative pressure $p_r(z)$. This term is decomposed into expressions for the mean relative and perturbation pressures

$$p_r = \frac{1}{2}[\epsilon] g\eta + g[\epsilon z] + \rho_s g\eta$$

$$p_r' = p_r - [p_r], \tag{10}$$

where $[\ ] = H^{-1}\int(\ )dz$ represents a vertical average, ϵ is the density deviation ($\rho - \rho_0$), η is the perturbation height of the ocean surface from a mean depth H and ρ_s is the ocean density near the surface.

The barotropic mode is treated separately in the momentum equations by dividing the current into a vertical mean and a perturbation. The vertical-mean pressure gradient force ($\partial[p_r]/\partial x$) exerts the same force throughout the water column and excites the vertical mean currents. The perturbations of the relative pressure gradient force ($\partial p_r'/\partial x$) excite the baroclinic part of the ocean response (Chang 1985). Since the free-surface height enters into the pressure terms, a prognostic equation for η has to be derived by assuming that $w = 0$ at $z = -H$ and vertically integrating the conservation of mass equation

$$\frac{\partial \eta}{\partial t} = -H\left(\frac{\partial [u]}{\partial x} + \frac{\partial [v]}{\partial y}\right) - \frac{\partial (u_s \eta)}{\partial x} - \frac{\partial (v_s \eta)}{\partial y}, \tag{11}$$

where u_s and v_s are the near-surface velocities. The magnitudes of the first two terms on the right side of (11) are about an order of magnitude larger than the last two terms.

The model is integrated forward in time using a leapfrog scheme and centered differencing in space with second-order accuracy (Chang 1985). As described above, there are two time steps: a 40 s time step for the barotropic integrations and a 1200 s time step for the baroclinic mode integration. The total time integration in the following simulations is 132 h or approximately 5 IP.

TABLE 2. Air/sea parameters used in the numerical model for hurricane Frederic.

R_{max} (km)	30
τ_{max} (Nt m^{-2})	3.3
U_h (m s^{-1})	6.5
h (m)	30
$g' \times 10^{-2}$ (m s^{-1})	2.2
b (m)	200
IP (d)	1.0
c_1 (m s^{-1})	3
Λ (km)	580
$S\ (U_h/2R_{max}f)$	1.4

d. Initial stratification

The model is initialized with a salinity–temperature–depth (STD) profile acquired in the northern Gulf of Mexico at the Mobile OTEC site in the summer of 1977 (Starr and Maul 1982). The maximum buoyancy frequency is 10 cph at 50 m, then decreases to about 2 cph over 250 m and is 1.5 cph below 400 m (Fig. 7). This profile closely resembles climatology and AXBT observations of Black (1983).

e. Mixing effects and bottom drag

In the Chang (1985) model, vertical mixing is parameterized using an eddy diffusivity K_z based on a mixing length (l_m) and the Richardson number (Ri)

$$K_z = \begin{cases} (1 - \mathrm{Ri})^{1/2}\left(\dfrac{\partial^2 u}{\partial z^2} + \dfrac{\partial^2 v}{\partial z^2}\right)^{1/2} l_m^2, & \mathrm{Ri} < 1, \\ 0, & \mathrm{Ri} > 1, \end{cases}$$

where the gradient Richardson number is defined as

$$\mathrm{Ri}(z) = \frac{N^2(z)}{u_z^2 + v_z^2}, \qquad (12)$$

and u_z and v_z represent the vertical shear of the current. Chang (1985) argues that this closure scheme produces better upwelling with the increased vertical resolution of the model. To save computation time, the mixing length is set to 30 m, which is the initial mixed layer depth and represents a rather large eddy scale. In a supplemental numerical experiment with l_m = 10 m, the model simulation after 24 h was very similar to that with l_m = 30 m. The vertical fluxes at the top and bottom boundaries of the ocean are assumed to be zero, except for the wind stress at the surface.

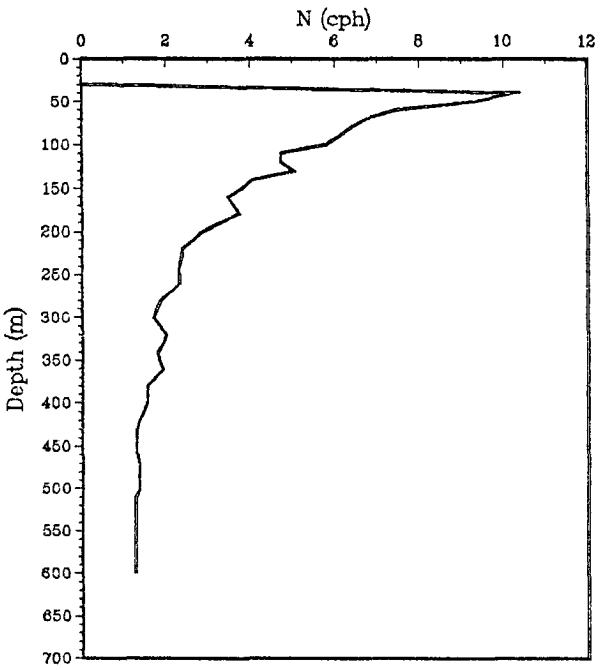

FIG. 7. Buoyancy frequency (cph) profile from an OTEC STD station 10 at 29°N, 88°W (Starr and Maul 1982).

The horizontal diffusion coefficient is defined as

$$K_h = \Delta^2 k_0^2 [D_1^2 + D_2^2]^{1/2},$$

where Δ is the horizontal grid interval, k_0 is the von Kármán constant (0.41) and D_1 and D_2 are the deformations

$$D_1 = \left(\frac{\partial u}{\partial x} - \frac{\partial v}{\partial y}\right), \quad D_2 = \left(\frac{\partial v}{\partial x} + \frac{\partial u}{\partial y}\right).$$

With maximum currents of 2 m s^{-1}, the maximum nondimensional horizontal diffusion coefficient $(K_h \Delta t)/(\Delta x \Delta y)$ is 5×10^{-3}. This small horizontal diffusion is sufficient to suppress computational instability that may exist in the numerical solution.

The effect of drag in the bottom layer is included by adding a Rayleigh friction term $-\lambda u$ and $-\lambda v$ to the $K_z(u)$ and $K_z(v)$. The value of λ is 2.3×10^{-6}, which corresponds to an e-folding scale of five days. With an 80 m bottom layer in the model, the bottom drag is about 30% stronger than used by Haidvogel and Brink (1986). In these numerical simulations, the ocean response is not very sensitive to the value of λ.

4. The simulated response

a. Horizontal structure

Maximum mixed-layer velocities of about 140 cm s^{-1} (Fig. 8) are to the right of the storm at about $x = 3R_{\max}$, which agree fairly well with the mixed-layer currents at CMA3 in hurricane Frederic (see Fig. 2). The rightward bias of the maximum current response has been attributed to nonlinear processes (Chang and Anthes 1978; Price 1983). On the right side of the track, the clockwise rotation of the velocity vector induces a strong divergence and convergence of mixed-layer currents. Based on linear theory (Geisler 1970), the wavelength of these divergent and convergent cells is 580 km ($U_h \times$ IP). Notice the wavelength appears to be decreasing in the wake which may be associated with the geostrophic adjustment process.

In the present simulations, the thermocline (285 m) currents are 180° out of phase with the mixed-layer current at $y = 0.5\Lambda$ (Fig. 8b). This phase reversal between the mixed-layer and thermocline currents indicates that the mixed layer is forced by the wind stress whereas the thermocline processes are driven by pressure gradient effects (Price 1983). As in the mixed layer, thermocline velocity vectors are elongated in the cross-track direction on both sides of the storm track, which indicates divergence and convergence. The maximum near-inertial currents are 30 cm s^{-1}, whereas the thermocline current response to a Frederic-type forcing in the rigid-lid model of Hopkins (1982) was about 10

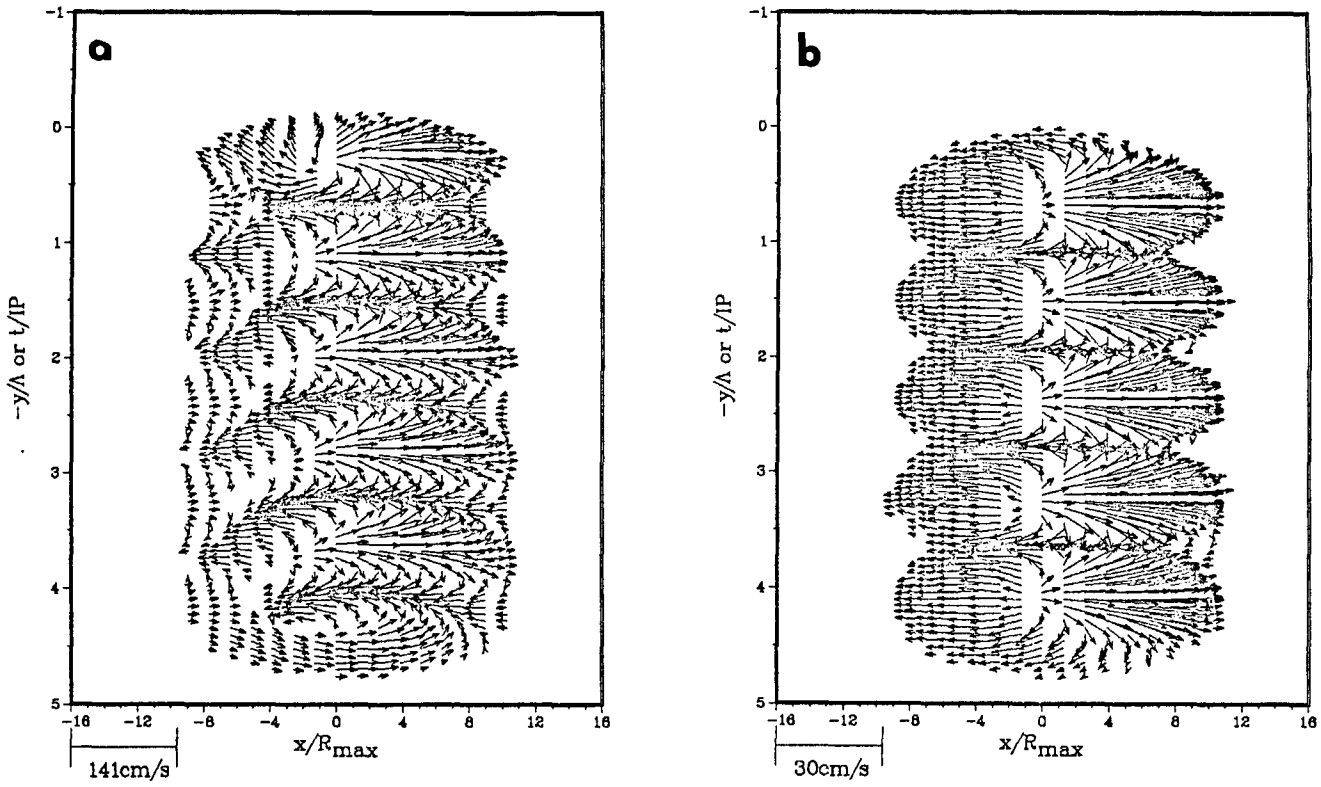

FIG. 8. Currents (cm s^{-1}) in (a) mixed layer and (b) thermocline (285 m) from the numerical model. The length of the vectors is proportional to the magnitude of the current according to the scale along the x-axis. The axes are scaled as in Fig. 3 with the storm center located at $x = 0$, $y = 0$.

cm s^{-1}. Thus, free-surface effects induce an almost immediate excitation of thermocline currents that are consistent with the observations (Fig. 2).

Maximum vertical velocities at 90 m and 225 m (Fig. 9) are 0.08 cm s^{-1} and 0.07 cm s^{-1}, which are consistent with the vertical velocity of 0.06 cm s^{-1} estimated from scale analysis ($\tau_{max}/\rho_0 U_h$) (Price 1983). Notice that the first cell of vertical velocity is upward and is followed by a cell of downward vertical velocity. In the wake, the alternating cells of upwelling and downwelling of water are found in the thermocline. After a few IP, the relative maxima of these cells is moving away from the storm track which is indicative of the horizontal dispersion of energy.

b. Along-track sections

The excitation of the ocean currents and temperatures throughout the water column is shown in the vertical cross sections along $x = 4R_{max}$ (Fig. 10). To emphasize upper-ocean processes, the vertical coordinate (ξ) is scaled using WKBJ theory

$$d\xi = (N(z)/N_0)dz, \qquad (13)$$

where N_0 is the vertically-averaged buoyancy frequency (1–2 cph). Because of the larger buoyancy frequency in the thermocline, the scaling stretches the grid spacing in the thermocline and shrinks it in the bottom layers.

Within the first IP ($y = \Lambda$), the cross-track currents are excited throughout the water column with a current reversal at about (stretched) 90 m (Fig. 10). According to (12), an increase in the vertical current shear decreases the Richardson number to below the critical value, which causes a mixing of heat and momentum (Pollard et al. 1973). As vertical mixing continues, the depth of the current reversal increases to a maximum of 200 m after an IP. The phase of the current slopes upward, which is associated with a downward propagation of energy (Leaman and Sanford 1976). This baroclinic process is evident in the increasing currents between 400–600 m depth, especially at $y = 4.5\Lambda$. Maximum thermocline velocities increase to 20–30 cm s^{-1} near 5 IP with a similar upward phase tilt of the velocity at $t = 1$ IP.

In the model, a rapid decrease in the mixed layer temperature occurs with 1–1.2°C maximum temperature changes following storm passage (Fig. 10) at $x = 4R_{max}$. The maximum decrease in mixed layer temperature (1.6°C) occurs at $x = 2R_{max}$ (not shown), which is consistent with observations (Black 1983). Along the track, the cooling and warming oscillation is associated with the upwelling and downwelling cycles induced by the divergence and convergence of upper

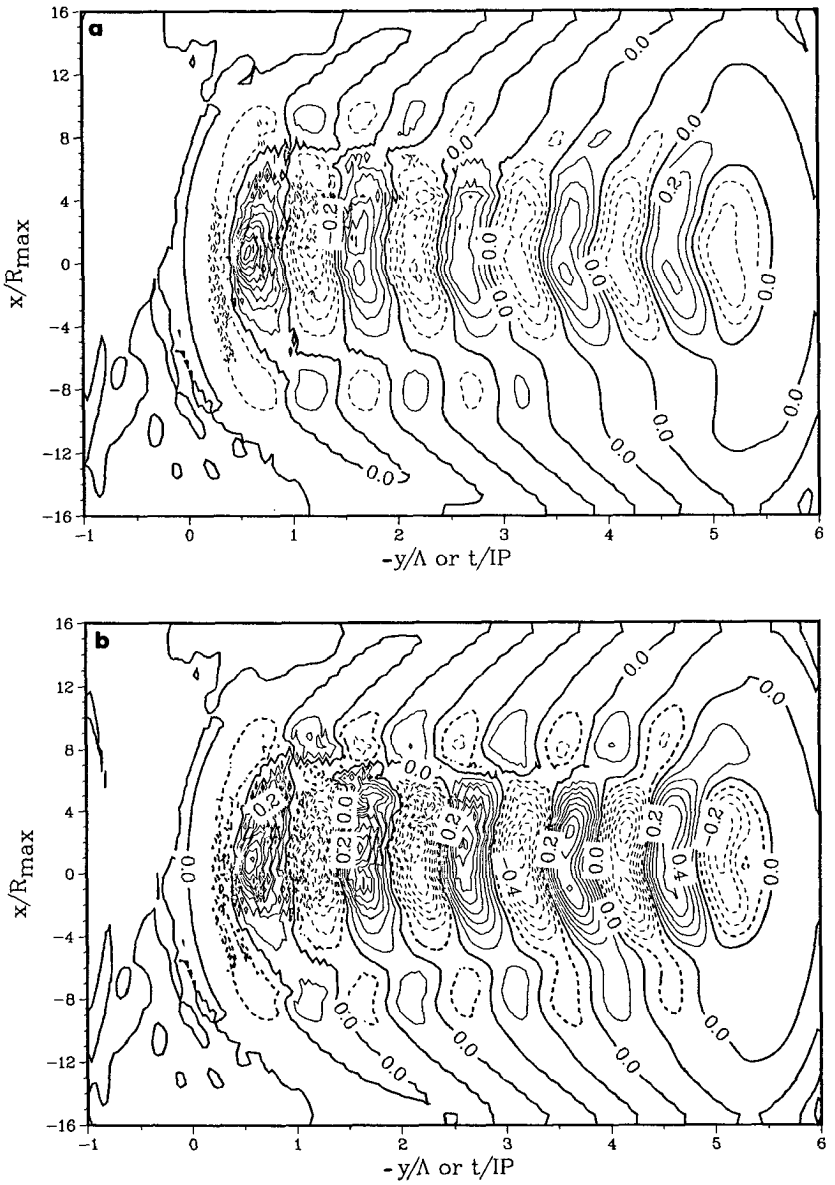

FIG. 9. Vertical velocities (cm s^{-1}) at (a) top of the thermocline (90 m) and (b) bottom of the thermocline (225 m) model. The solid (dashed) contours represent upward (downward) motion at an interval of 0.1 cm s^{-1} relative to the maximum values of 8×10^{-2} cm s^{-1} (90 m) and 7×10^{-2} cm s^{-1} (225 m). The axes are scaled as in Fig. 3 with the storm center at $x = 0$, $y = 0$.

ocean currents. Farther from the storm center, horizontal advection of temperature gradients also cause a warming and cooling cycle. Downward fluxes of heat from the mixed layer induce a warming of the thermocline between 50–200 m. The bottom of the temperature oscillation coincides with the zone of enhanced vertical current shear.

c. *Effects of the free surface*

In this section, key physical mechanisms that could not be resolved by the analytical model will be isolated. This allows for a more complete description of free-surface effects on the oceanic wake during and subsequent to the passage of a hurricane.

The three-dimensional and plan views of the free-surface depression (Fig. 11) illustrates the barotropic trough described by Geisler (1970) plus a longer wavelength oscillation. The maximum surface depression of 20 cm is located along the storm track at $y \sim 0.5\Lambda$. The relative maxima in the surface depression are modulated by the near-inertial cycle. These free-surface oscillations have amplitudes of about 4–6 cm as in the

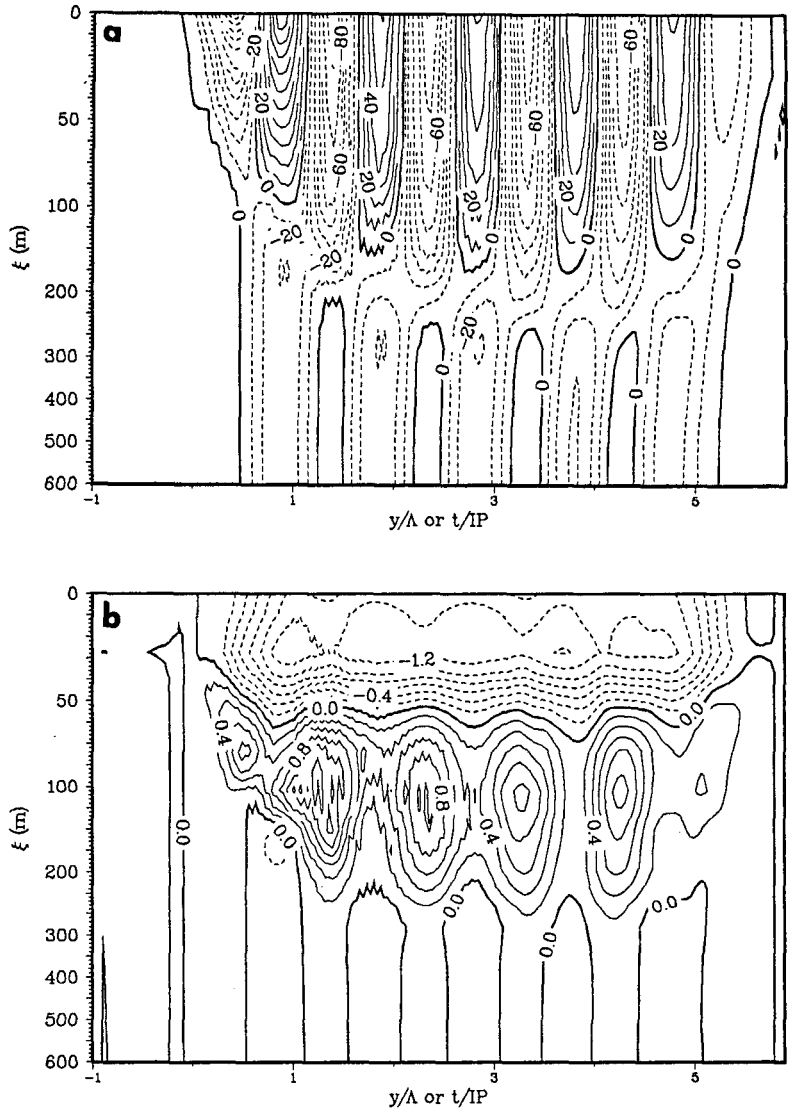

FIG. 10. (a) Cross-track component of current (cm s^{-1}) from the numerical model at $x = 4R_{max}$ with positive (negative) components depicted as solid (dashed) contours at an interval of 10 cm s^{-1}. (b) Temperature increases (decreases) are indicated by solid (dashed) contours with an interval of 0.2°C. The abscissa is scaled by the near-inertial wavelength Λ (580 km) and depth (ξ) is WKBJ-stretched.

simulations by Cooper and Thompson (1989). Although the free surface is also depressed by 22 cm in the analytical model simulation, the surface depression is elongated in the along-track direction, which may be due to nonlinear processes in the numerical model.

A larger scale wave in the free surface depression excited by the hurricane extends over the domain. This longer period oscillation, with maximum amplitudes of 2 cm, has a wavelength of approximately (2Λ) 1060 km. As shown in Table 1, the barotropic deformation radius in a 610 m ocean is 1092 cm which is within 30 km (1–2 grid intervals) of the wavelength of this larger barotropic wave. Thus, the relevant scale appears to the barotropic deformation radius instead of the free wave wavelength of O(10^4 km).

According to (10), the spatial deformation in the free surface induces a change in the vertical mean pressure gradient, which excites ocean currents throughout the water column. The negative and positive centers of the depth-averaged vertical velocity (Fig. 12) are associated with a net divergence and convergence of the depth-averaged currents. A maximum depth-averaged vertical velocity of 8×10^{-4} cm s^{-1} occurs slightly to the right of the storm track at about $x = 1R_{max}$. Although the initial wavelength of the cells is about 580 km, the wavelength decreases by few per-

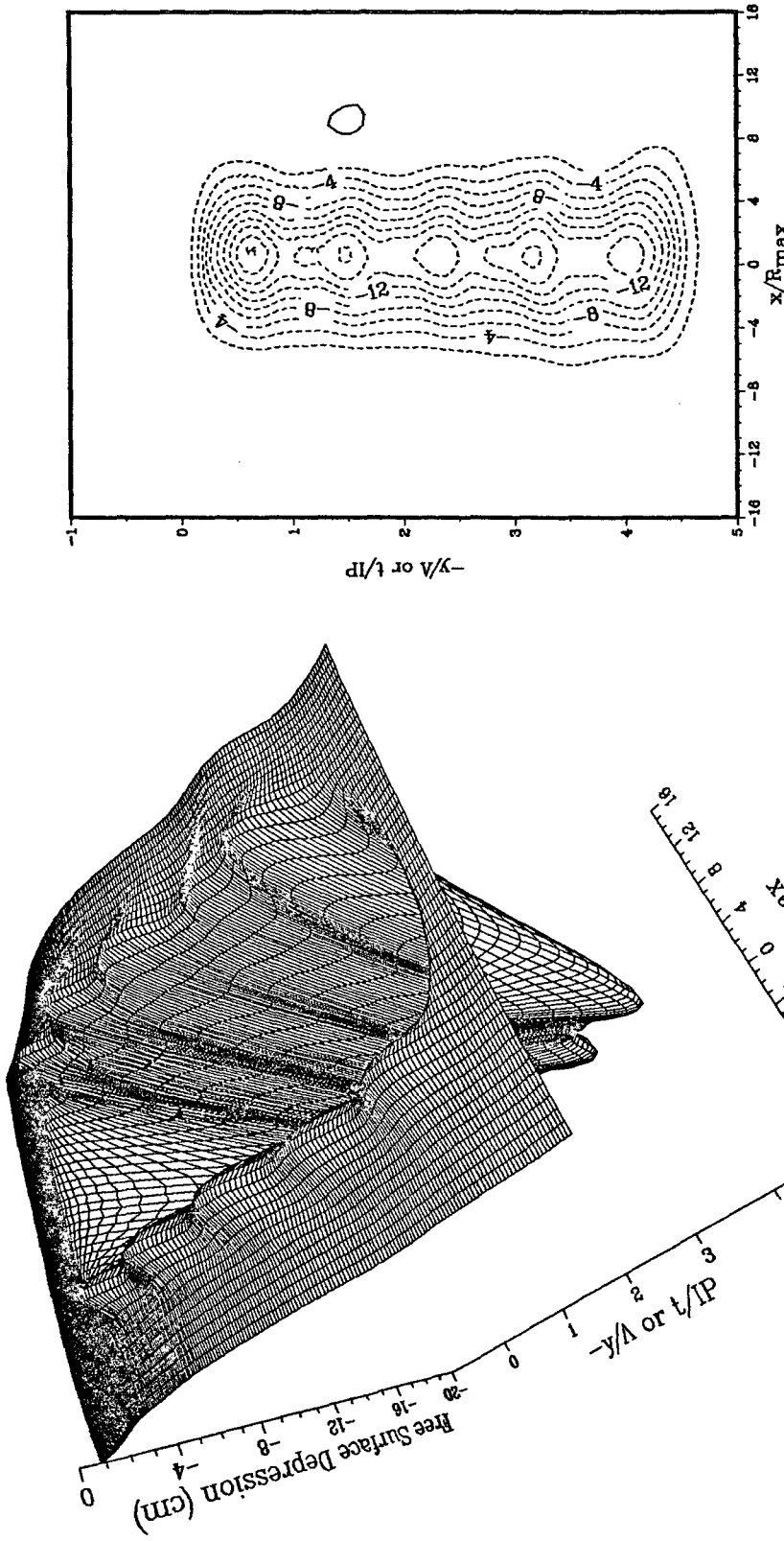

FIG. 11. Three-dimensional (left panel) and plan (right panel) views of deviations in the free surface height (cm) relative to an undisturbed height simulated by the numerical model. The axes are scaled as in Fig. 3.

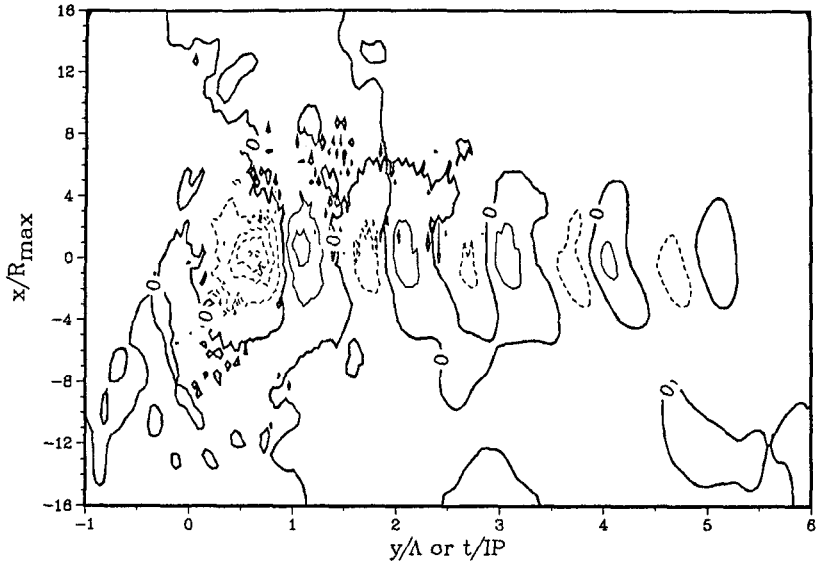

FIG. 12. Vertical velocity at surface evaluated by vertically-integrating the conservation of mass equation over depth. The solid (dashed) contours represent upward (downward) motion with contour interval of 2×10^{-4} cm s^{-1}. The axes are scaled as in Fig. 3.

cent in the wake of the hurricane. Because of the shortness of the record (5 IP), the rate of damping cannot be accurately determined.

To assess the contribution of the free surface slope on the ocean current simulations, the velocities (including geostrophic and near-inertial) are calculated from the gradient of the free surface depression (Fig. 13). On the right (left) side of the track, the maximum along-track components are 12–14 cm s^{-1} in the direction of (opposite to) the storm movement. A time-dependent velocity with an along-track wavelength of 580 km also appears to be present within $y = \pm 6R_{max}$. The maximum cross-track velocities (Fig. 13) are slightly weaker at 4–8 cm s^{-1} with similar wavelengths of 580 km. Since these velocity components contain both the geostrophic and near-inertial contributions, the maximum is at a different location than the analytical model simulations of the near-inertial response in Fig. 4. The reason for this difference is due to the geostrophic component, which is subtracted from (7) of the analytical model.

5. Near-inertial current analysis

Since the simulations from the primitive equation model have many of the observed and modeled features shown in previous studies, they appear to have sufficient veracity to justify a comparison with the Frederic observations. In particular, the free-surface model allows for a deeper penetration of the hurricane-induced current response and an excitation of near-inertial motions than rigid lid models. In this section, the analysis of the simulations is focused on the response in the near-inertial wave band.

a. Frequency analysis

Price (1983) showed that the frequency shift of near-inertial motions above the local Coriolis parameter f depends on the mixed-layer (M) Burger number

$$\mathrm{M} = \frac{(1 + 1/S^2)g'h}{(2R_{\max}f)^2},$$

where S is the nondimensional storm speed ($U_h/2R_{\max}f$), h is the mixed layer depth, and g' is the reduced gravity (values of the parameters are given in Table 2). The Burger number M measures the importance of the horizontal pressure gradient that couples the mixed layer to the thermocline. The shift in the frequency above the local inertial frequency is equal to M/2, or approximately $1.03f$ in the model simulations.

The simulated horizontal velocities at each model level are fit to a series of trial frequencies (0.9–$1.2f$) to diagnose the frequency of the oscillations over a 5 IP segment at $x = 3R_{\max}$ (Mayer et al. 1981). The carrier frequency is defined to be the frequency that minimizes the covariance of the residual signals. The diagnosed frequencies are blue-shifted between 1%–6% above the local inertial frequency. This blue-shift in the frequency is evident in the upper ocean as the carrier frequency slowly changes from $1.01f$ at the surface (5 m) to about 1.04–$1.05\ f$ at 135 m. The analytical model accounts for about 80% of the mixed layer variance between 1.02 to 1.03 f and for over 60% of the simulated current variability in the upper part of the thermocline. The mixed-layer Burger number of $1.03f$ agrees with the diagnosed carrier frequency in the mixed layer.

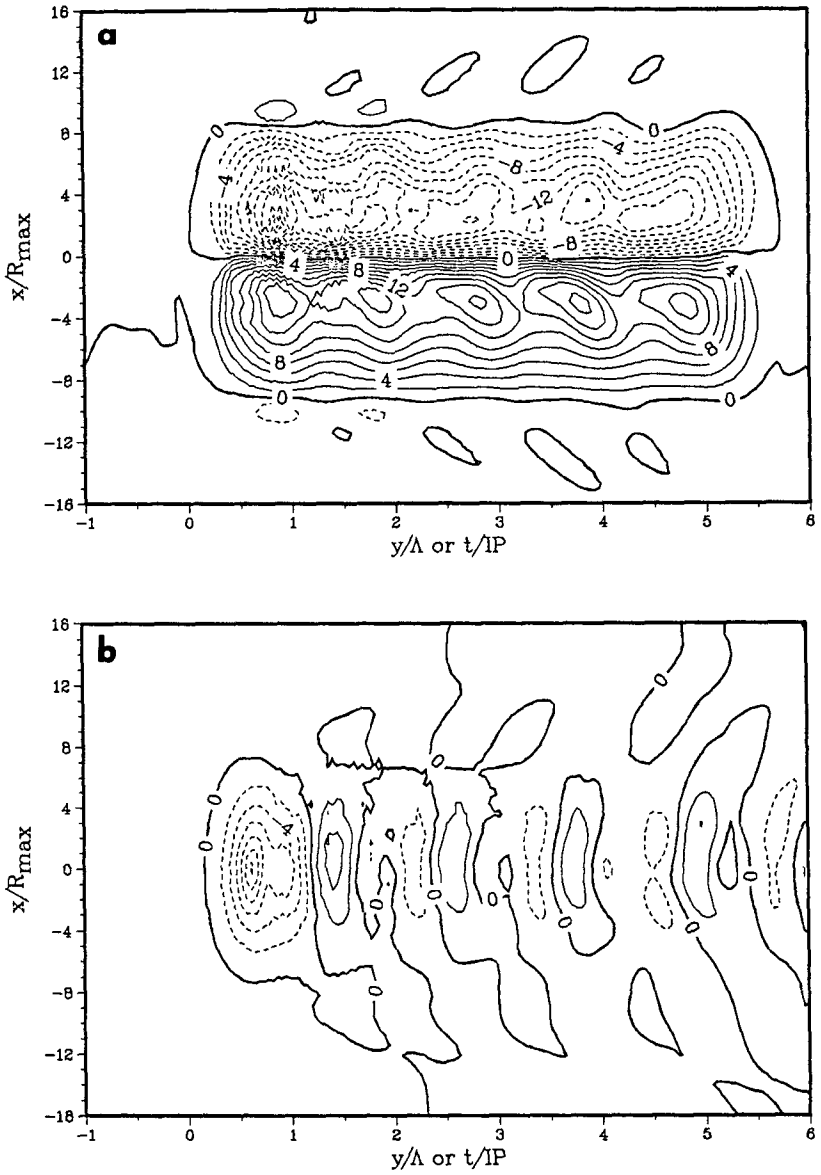

FIG. 13. (a) Along-track and (b) cross-track current components associated with the sea-surface depression in Fig. 11. The solid (dashed) contours represent positive (negative) values at a contour interval of 2 cm s^{-1}. The axes are scaled as in Fig. 3.

b. CW-rotating currents

The simulated velocity data are demodulated at a carrier frequency of $1.03f$ to isolate the near-inertial response. The technique is similar to that used in SE except that the data are filtered using a running inertial period mean because the simulated time series only extends 5 IP. Since the demodulation process yields four amplitudes (cosine and sine for each velocity component), the CW-rotating amplitudes can be obtained following Mooers (1973). The motivation here is to show that there is a strong baroclinic and a significant barotropic current in the near-inertial wave band in the numerical simulations.

Vertical cross sections of the normalized CW-rotating amplitudes and phases are shown in Fig. 14 at 1.5 and 4.5 IP following the passage of the model storm. The maximum mixed-layer currents of about 120 cm s^{-1} are located at $x = 2R_{max}$, indicative of the rightward bias in the numerical model. The velocity amplitude decreases to 20–30 cm s^{-1} across the enhanced shear zone between 75–100 m. Near-inertial amplitudes are about 10 cm s^{-1} from 100–600 m. Although the CW-rotating phase indicates a half-cycle difference between

the mixed layer and thermocline current response, only small phase differences occur between the thermocline and near-bottom levels. Thus, the initial response is a larger baroclinic component superposed on a smaller barotropic component. The initial current amplitudes simulated by rigid-lid baroclinic models are smaller at depth (Hopkins 1982).

After 4.5 IP, maximum current amplitudes in the mixed layer are about 60 cm s^{-1} (Fig. 14b). The 10 cm s^{-1} velocity in the upper part of the thermocline from 90 m at $t = 1.5$ IP has been displaced to 200 m. Significant amplitudes extend from $-4R_{max} < x < 6R_{max}$ which indicates the dispersion of waves away from the track as part of the evolving, three-dimensional response. The phases in the thermocline and bottom layers are separating, which implies upward phase propagation (Leaman and Sanford 1975).

The simulated CW-rotating amplitudes of mixed layer velocities agree fairly well with the Frederic observations (SE) at about $x = 3R_{max}$ (Fig. 15a). The maximum observed velocity amplitude is 90 cm s^{-1} compared to a simulated amplitude of 100 cm s^{-1}. The simulated amplitudes begin to decrease after only 0.5 IP and decay over an e-folding time scale of 4–5 IP. By contrast, the observed current amplitudes remain constant over the first 2 IP and then exponentially decrease. In the thermocline (250 m), the simulated amplitude has an initial maximum of 20 cm s^{-1} compared to an observed amplitude of 26 cm s^{-1}. The current amplitudes agree within ± 2 cm s^{-1} ($\sim 10\%$ of the signal) after $t = 1.5$ IP. However, the simulations of the thermocline currents by the rigid-lid model of Hopkins (1982) were about a factor of two less than the Frederic observations and the simulations here. Initially, the observed and simulated near-bottom currents agree fairly well with amplitudes of 18 cm s^{-1}. After 2 IP, the effects of the bottom topography appear to be dominating the near-bottom (435 m) response (Lai and Sanford 1986). Even in a model with bottom topography (Cooper and Thompson 1989), correlation coefficients between the observed and simulated currents were about 0.5 which suggests complicated dynamics close to the ocean bottom.

As shown in Fig. 15b, there is good agreement between the phases of the observed and simulated current amplitudes. Although the phases vary rapidly in time in the thermocline and bottom layers during the first 2 IP, the phase shifts with depth remain constant afterward. Phase changes in time suggests that the frequency of the forced oscillations may be changing slightly (Pedlosky 1979). In a response that contains both barotropic and baroclinic components, the dispersion of the waves from the forced regime may cause variations in the phase during the first few IP.

c. *Barotropic current response*

The simulated barotropic current is calculated by vertically-averaging the real part of the CW-rotating current amplitude as in SE (Fig. 16). The spatial pattern of amplitudes is similar to the magnitudes of the barotropic current simulated by the analytical model (see Fig. 4). In particular, maximum amplitudes of the barotropic current along $x = 3R_{max}$ exceed 10 cm s^{-1}, which agrees well with the calculations at CMA3 by SE. Although the time series is short, the amplitudes decay gradually downstream, which is consistent with the observations and linear theory ($1/\sqrt{y\alpha_0}$). One difference in the numerical model is that the lateral extent of the barotropic current response extends farther to the left and right of the track than in the linear simulations.

Differences (Fig. 17) between the analytical (in Fig. 4) and the numerical (Fig. 16) model simulations are less than 2 cm s^{-1} between $0 < x < 4R_{max}$. This small residual indicates that a large part of the barotropic response in the near-inertial wave band is linear. The larger residual amplitudes (>2 cm s^{-1}) on the left ($-4R_{max} < x < 0$) and on the right side ($4R_{max} < x < 8R_{max}$) of the storm track are due to the larger amplitudes simulated by the numerical model. The analytical model simulation of the cross-track current may be damping too rapidly compared to the cross-track component simulated by the numerical model. These larger residual amplitudes on the periphery may also be associated with nonlinear processes in the numerical model. Another possible explanation is that the actual forcing in the analytical model is confined to too small a domain compared to the numerical model.

6. Conclusions

The original motivation for this study was to determine if the observed depth-averaged current in hurricane Frederic in Shay and Elsberry (1987) was associated with free-surface effects, rather than being an artifact of limited vertical sampling. However, the question of the barotropic ocean response to hurricanes is of more general interest. A linear model capable of simulating a barotropic response in the near-inertial wave band has been developed. The wind stress curl and divergence depress the sea surface to form a barotropic trough (Geisler 1970). The vertical mean pressure gradient associated with the sea-surface depression excites vertical mean currents. The net divergence and convergence of these currents then modulates the surface depression on near-inertial time scales.

The sea-surface depression may be simulated analytically by convolving a modified Bessel function with the wind stress curl and divergence. In the steady state, the sea surface slope induces a geostrophic current. To solve for the time-dependent current, the forced shallow water equations are transformed and inverted to find a second Green's function. The barotropic current oscillations are simulated from a convolution of the gradients of the sea-surface slope with the Green's function.

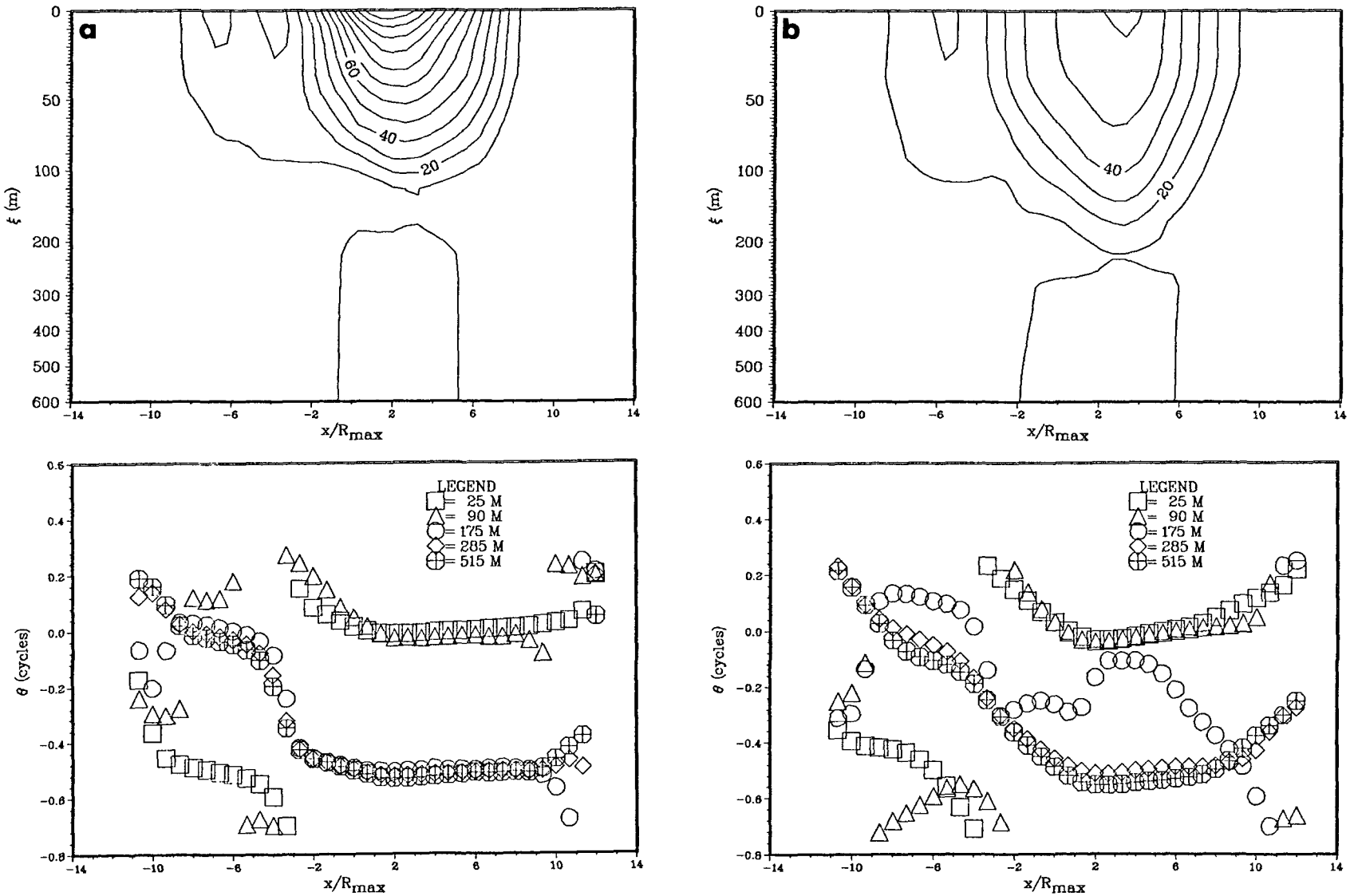

FIG. 14. Cross sections of CW-rotating amplitudes (cm s^{-1}) and phases (cycles) at (a) t = 1.5 IP and (b) t = 4.5 IP. The contour interval is 10 cm s^{-1} and the phases at 25 m (box), 90 m (triangles), 175 m (circles), 285 m (squares) and 515 m (circle plus) are calculated relative to the mixed-layer amplitude at x = 0. The depth (ξ) is WKBJ-scaled using (13) and the abscissa is scaled by R_{max}.

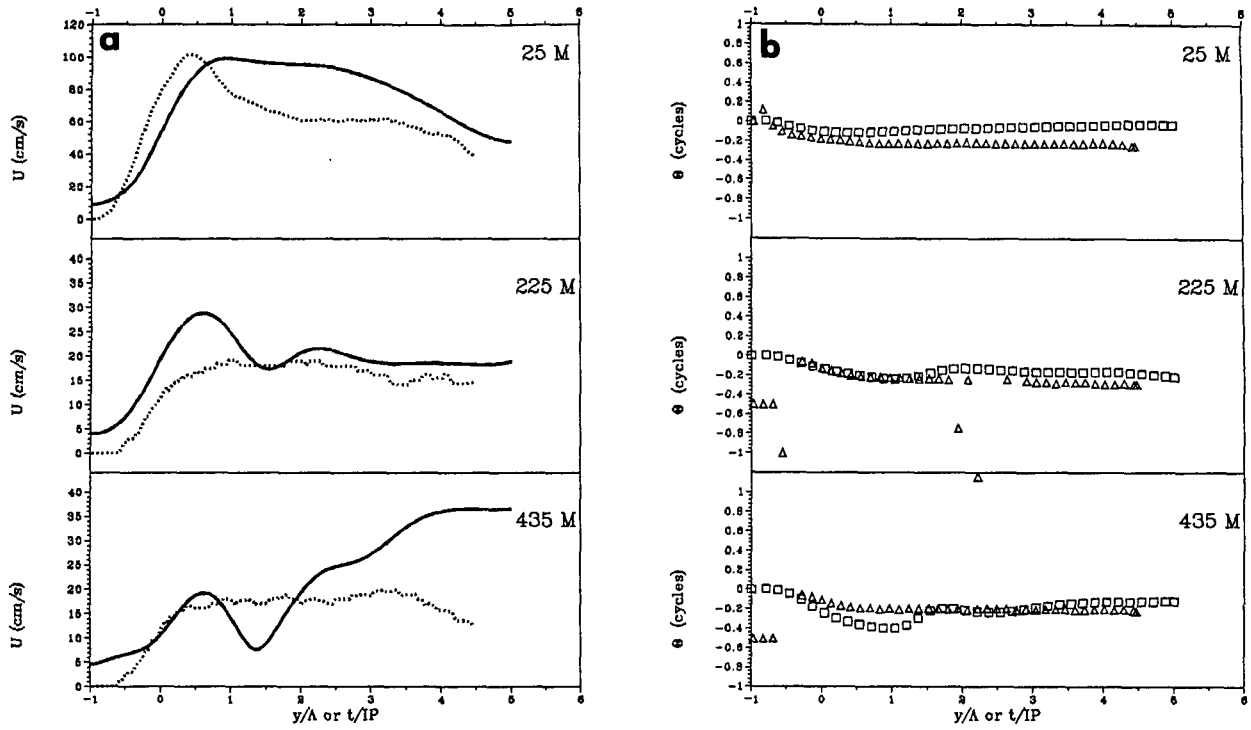

FIG. 15. (a) Observed (solid) and numerically simulated (dashed) CW-rotating amplitudes (cm s^{-1}); and (b) observed (box) and simulated (triangle) phases (cycles) in the mixed layer (25 m), thermocline (225 m) and near-bottom (435 m) at $x = 3R_{max}$. Phase is computed relative to the mixed layer at $y = 0$ and the abscissa is scaled by Λ.

These barotropic oscillations have a wavelength ($U_h \times$ IP) similar to the baroclinic wavelength in the wake of a moving hurricane. The shift in wavelength and frequency is proportional to $(1 - U_h^2/c_0^2)^{-1/2}$, which is approximately 1% above f. Maximum amplitudes of the barotropic current decrease from about 20 cm s^{-1} in a 300-m deep ocean to 2–3 cm s^{-1} in a 4000 m deep ocean. Maximum currents are displaced to the right of the storm track by $2R_{max}$ and decay downstream as $1/\sqrt{y\alpha_0}$, which is similar to the baroclinic response (Geisler 1970). In a 610-m deep ocean, the simulated initial amplitudes of the barotropic current at $x = 3R_{max}$ are about 10–11 cm s^{-1} which is comparable with the 9–11 cm s^{-1} observed depth-averaged currents from hurricane Frederic. Over about 4–5 IP, the simulated barotropic amplitude is within 2 cm s^{-1} of the observed depth-averaged current and suggests that the rate of decay in the model is consistent with the observational evidence (SE). Consequently, it is concluded that a barotropic current in the near-inertial waveband was excited by the passage of hurricane Frederic.

A free surface has been incorporated in a multi-level, three-dimensional primitive equation model capable of simulating the combined barotropic and baroclinic response of a moving hurricane. The simulations of ocean currents and temperatures contain many of the features that have been previously observed (Black 1983) and modeled (Chang and Anthes 1978; Price 1983). The predominant feature is the rightward enhancement of the maximum current and temperature response that oscillates over near-inertial wavelengths (Λ). The maximum observed mixed-layer currents of 120–140 cm s^{-1} are simulated fairly well by the model. The vertical velocity and temperature simulations indicate regions of upwelling and downwelling associated with the divergence and convergence of upper ocean currents with a near-inertial wavelength. The alternating cells of positive and negative vertical velocities spread laterally in the wake as a result of energy dispersion. Intermittent mixing occurs in the model via Richardson number instabilities as a result of enhanced vertical shear between the mixed layer and thermocline current.

Some marked differences are observed in the thermocline response compared to previous model studies (Hopkins 1982; Price 1983). Thermocline currents are excited almost immediately to a maximum of about 30 cm s^{-1}, which is comparable to the current meter observations (see Fig. 2). In the rigid lid model of Hopkins (1982), the thermocline currents were 50% smaller than the observed currents and delayed by 0.5 IP. Thus, inclusion of the free surface in the numerical model contributes to the realism of simulations of the

wake of a moving hurricane by allowing geostrophic and near-inertial velocities throughout the water column. There is also a larger scale barotropic wave excited by the hurricane that has an amplitude of 2 cm s^{-1} and a wavelength proportional to the barotropic deformation radius of 1090 km.

The near-inertial response is isolated from the numerical simulations by determining the carrier frequency of the forced waves and demodulating the current at $1.03f$ (Otnes and Enochson 1978). The Fourier coefficients are combined to form CW-rotating amplitudes and phases (Mooers 1973). The depth-averaged amplitude is about 10 cm s^{-1} compared to 9–11 cm s^{-1} derived from the observations. The evolution and downstream decay also agrees with both observations and analytical solutions. The spatial patterns of the barotropic amplitudes simulated by the analytical and numerical models are highly correlated, which suggests that the barotropic current response in the near-inertial wave band is governed by linear dynamics.

Based on the combination of observations with simulations from analytical and numerical models, it is concluded that hurricane Frederic excited a significant barotropic current within the near-inertial wave band in water depths of about 600 m. As noted in SE, the near-inertial wave wake of hurricane Frederic contained energetic baroclinic components and a significant barotropic current that is not just an artifact of limited vertical sampling. This barotropic response associated with free-surface effects can indeed contribute to the ocean current variability for the first few IPs following hurricane passage.

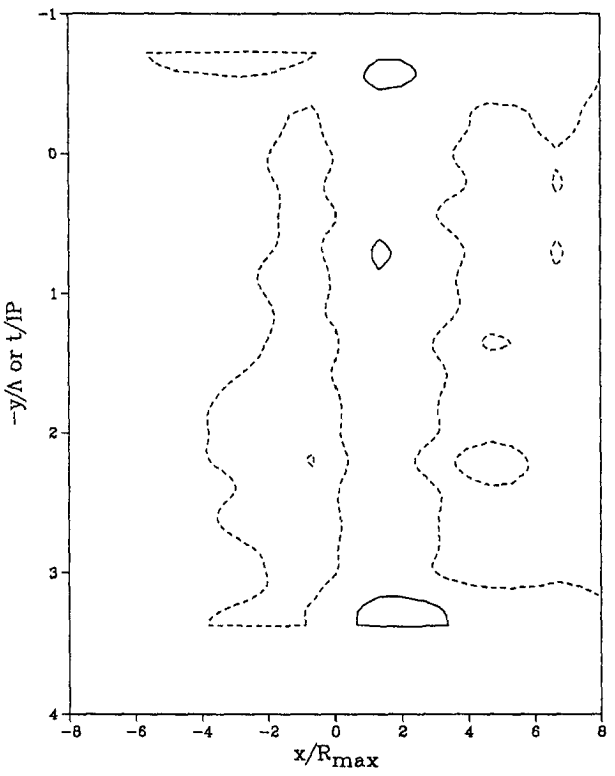

FIG. 17. Difference in the barotropic amplitudes between the linear analytic and numerical models. The contour interval is 2 cm s^{-1} and the axes are scaled as in Fig. 3.

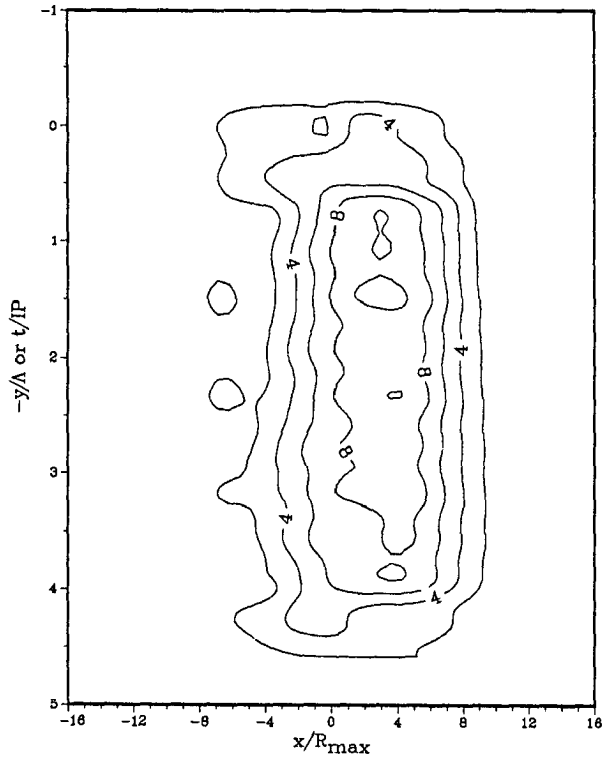

FIG. 16. Amplitudes (cm s^{-1}) of the demodulated velocities simulated from the primitive equation model simulations for the barotropic mode. The axes are scaled as in Fig. 3 with storm center at (0, 0).

Aknowledgments. The authors would like to thank the Current Meter Group (specifically Chuck Robinson, Jose Alonso and Steve Clark) of the Naval Oceanographic Office for providing the current meter observations acquired during Frederic. Comments by Bob Haney, Bill Garwood, Ed Thornton, Terry Williams and Art Schoenstadt of the Naval Postgraduate School are appreciated. We extend our appreciation to the two anonymous reviewers for their helpful comments. This research was sponsored of the Office of Naval Research (Ocean Science) and the Naval Postgraduate School. The numerical simulations were performed at the Naval Research Laboratory. Computer support for this research has been provided by the Church Computer Center of the Naval Postgraduate School and the Rosenstiel School of Marine and Atmospheric Science Computing Facility. The authors would like to extend our gratitude to Dennis Mar of the Church Computer

Center for help with the graphics. Mrs. Lila Ptak typed and revised the manuscript with remarkable patience.

REFERENCES

Anderson, D. L. T., and A. E. Gill, 1979: Beta-dispersion of inertial waves. *J. Geophys. Res.*, **84,** 1836–1842.

Beardsley, R. C., W. Boicourt, L. C. Huff and J. Scott, 1981: CMICE 76: A near surface current meter intercomparison experiment. *Deep-Sea Res.*, **28A,** 1577–1603.

Black, P. G., 1983: Ocean temperature changes induced by tropical cyclones. Ph.D. dissertation. The Pennsylvania State University, 278 pp.

Brink, K. H., 1989: Observations of the response of the thermocline currents to a hurricane. *J. Phys. Oceanogr.*, **19,** 1017–1022.

Brooks, D., 1983: The wake of hurricane Allen in the western Gulf of Mexico. *J. Phys. Oceanogr.*, **13,** 117–129.

Chang, S. W., 1985: Deep ocean response to hurricanes as revealed by an ocean model with a free-surface. Part I: Axisymmetrical case. *J. Phys. Oceanogr.*, **15,** 1847–1858.

——, and R. A. Anthes, 1978: Numerical simulations of the ocean's nonlinear, baroclinic response to translating hurricanes. *J. Phys. Oceanogr.*, **8,** 468–480.

Cooper, C., and J. D. Thompson, 1989: Hurricane-generated currents on the outer continental shelf Part 1: Model formulation and verification. *J. Geophys. Res.*, **94,** 12 513–12 540.

Erdelyi, A., W. Magnus, F. Oberhettinger and F. G. Tricomi, 1954: *Tables of Integral Transforms,* Vol. I, McGraw-Hill, 391 pp.

Geisler, J. E., 1970: Linear theory on the response of a two layer ocean to moving hurricane. *Geophys. Fluid Dyn.*,**1,** 249–272.

Gill, A. E., 1982: *Atmosphere-Ocean Dynamics.* Academic Press, 662 pp.

——, 1984: On the behavior of internal waves in the wakes of storms. *J. Phys. Oceanogr.*, **14,** 1129–1151.

Greatbatch, R. J., 1983: On the response of the ocean to a moving storm: The nonlinear dynamics. *J. Phys. Oceanogr.*, **13,** 357–367.

Haidvogel D., and K. H. Brink, 1986: Mean currents driven by topographical drag over the continental shelf and slope. *J. Phys. Oceanogr.*, **16,** 2159–2171.

Haltiner, G. J., and R. T. Williams, 1980: *Numerical Prediction and Dynamic Meteorology.* John Wiley and Sons, 477 pp.

Hebert, P., 1979: Preliminary report: Hurricane Frederic Aug. 29–Sept. 14, 1979. NOAA, National Hurricane Center, 10 pp.

Hopkins, C., 1982: Ocean response to hurricane forcing. M.S. thesis, Naval Postgraduate School, 89 pp.

Ichiye, T., 1976: Barotropic disturbances caused by a point storm in a β-plane ocean—Part I: Asymptotic analysis. *J. Oceanogr. Soc. Jpn.*, **32,** 33–47.

Kajiura, K., 1958: Response of a boundless two-layer ocean to atmospheric disturbances. Ph.D. dissertation, Agricultural and Mechanical College of Texas, College Station, Texas, 138 pp.

Kuo, H. H., and T. Ichiye, 1977: A numerical study of the response of a barotropic ocean to a moving hurricane. *Tellus,* **29,** 561–571.

Kundu, P. K., and R. E. Thomson, 1985: Inertial oscillations due to a moving front. *J. Phys. Oceanogr.*, **15,** 1076–1084.

Lai, D. Y., and T. B. Sanford, 1986: Observations of hurricane generated slope modes. *J. Phys. Oceanogr.*, **16,** 657–666.

Leaman, K. D., and T. B. Sanford, 1976: Vertical energy propagation of inertial waves: A vector spectral analysis of velocity profiles. *J. Geophys. Res.*, **80,** 1975–1978.

Lighthill, M. J., 1967: On waves generated in dispersive systems by travelling forcing effects with applications to the dynamics of rotating fluids. *J. Fluid. Mech.*, **27,** 725–752.

Mayer, D., M. O. Mofjeld and K. D. Leaman, 1981: Near-inertial internal waves on the outer shelf in the middle Atlantic Bight in the wake of hurricane Belle. *J. Phys. Oceanogr.*, **11,** 86–106.

Mooers, C. N. K., 1973: A technique for the cross-spectrum analysis of complex valued time series with emphasis on properties of polarized components and rotational invariants. *Deep-Sea. Res.*, **20,** 1129–1141.

Otnes, R. K., and L. Enochson, 1978: *Applied Time Series Analysis.* Wiley-Interscience, 449 pp.

Pedlosky, J., 1979: *Geophysical Fluid Dynamics.* Springer-Verlag, 625 pp.

Pollard, R. T., 1970: On the generation by winds of inertial waves in the ocean. *Deep-Sea Res.*, **17,** 795–812.

——, P. B. Rhines and R. Thompson, 1973: The deepening of the wind mixed layer. *Geophys. Fluid Dyn.*, **3,** 381–404.

Price, J. F., 1981: Upper ocean response to a hurricane. *J. Phys. Oceanogr.*, **11,** 153–175.

——, 1983: Internal wave wake of a moving storm. Part I: Scales, energy budget and observations. *J. Phys. Oceanogr.*, **13,** 949–965.

Sanford, T. B., P. G. Black, J. Haustein, J. W. Fenney, G. Z. Forristall and J. F. Price, 1987: Ocean response to hurricanes. Part 1: Observations. *J. Phys. Oceanogr.*, **17,** 2065–2083.

Schoenstadt, A. L., 1977: The effect of spatial discretization on the steady state and transient behavior of the dispersive wave equation. *J. Comput. Phys.*, **23,** 364–379.

Shay, L. K., and R. L. Elsberry, 1987: Near-inertial ocean current response to hurricane Frederic. *J. Phys. Oceanogr.*, **17,** 1249–1269.

——, —— and P. G. Black, 1989: Vertical structure of the ocean current response to a hurricane. *J. Phys. Oceanogr.*, **19,** 649–669.

Starr, R. B., and G. A. Maul, 1982: Physical oceanographic observations in the eastern Gulf of Mexico 1979–1980 for a potential OTEC Site. NOAA Tech. Memo. ERL-AOML-50, Atlantic and Meteorological Laboratories, 205 pp.